

***Title Page***

**Intravitreal injection of AAV2 transduces macaque inner retina**

Lu Yin<sup>1,2</sup>, Kenneth Greenberg<sup>4,5,6</sup>, Jennifer J. Hunter<sup>1</sup>, Deniz Dalkara<sup>4</sup>, Kathleen D. Kolstad<sup>4,5,6</sup>, Benjamin D. Masella<sup>3</sup>, Robert Wolfe<sup>2</sup>, Meike Visel<sup>4,5,6</sup>, Daniel Stone<sup>4,7</sup>, Richard T. Libby<sup>1,2</sup>, David DiLoreto Jr.<sup>1</sup>, David Schaffer<sup>4,7</sup>, John Flannery<sup>4,5,6</sup>, David R. Williams<sup>2,3</sup>, William H. Merigan<sup>1,2</sup>

Flaum Eye Institute<sup>1</sup>, Center for Visual Science<sup>2</sup>, Institute of Optics<sup>3</sup>, University of Rochester, Rochester, NY, USA

Helen Wills Neuroscience Institute<sup>4</sup>, Department of Molecular and Cell Biology<sup>5</sup>, Department of Vision Science<sup>6</sup>, Department of Chemical Engineering<sup>7</sup>, University of California, Berkeley, CA, USA

Correspondence should be addressed to W.H.M. (billm@cvs.rochester.edu)

§Corresponding author:

William H. Merigan

Department of Ophthalmology and Center for Visual Sciences

Rochester, NY 14642

Tel: 585-275-4872

FAX: 585-473-3411

billm@cvs.rochester.edu

Short title: AAV2 transduction in macaque inner retina

Word count: Abstract, 249 words; Text, 4578 words

Grant information: see *Acknowledgements*

**Abstract**

**Purpose:** Adeno-associated virus serotype 2 (AAV2) has been shown to be effective in transducing inner retinal neurons, following intravitreal injection in several species. However, results in non-primates may not be predictive of transduction of human inner retina, because of differences in eye size and the specialized morphology of the high acuity human fovea. Here we studied inner retina transduction in the macaque, a primate with ocular characteristics most similar to human.

**Methods:** *In vivo* imaging and histology was used to examine GFP expression in macaque inner retina following intravitreal injection of AAV vectors containing five distinct promoters.

**Results:** We found that AAV2 produced pronounced GFP expression in inner retinal cells of the fovea, no expression in central retina beyond the fovea, and variable expression in peripheral retina. AAV vector incorporating a neuronal promoter, human connexin 36 (hCx36), transduced ganglion cells within a dense annulus around the fovea center, whereas AAV2 containing a ubiquitous promoter, hybrid cytomegalovirus (CMV) enhancer/chicken- $\beta$ -actin (CBA), transduced both Müller and ganglion cells in a dense circular disc centered on the fovea. With three shorter promoters - human synapsin (hSYN), and the shortened CBA and hCx36 promoters (smCBA and hCx36sh), AAV2 only produced visible transduction as seen in fundus images, when the retina was altered by ganglion cell loss or enzymatic vitreolysis.

**Conclusion:** These results in macaque suggest that intravitreal injection of AAV2 will produce high levels of gene expression at the human fovea, important for retinal gene therapy, but not in central retina beyond the fovea.

## **Introduction**

Viral-mediated gene delivery has been extensively studied for retinal transduction<sup>1,2</sup> for basic research<sup>e.g.,<sup>3</sup></sup>, and clinical applications<sup>e.g.,<sup>4,5</sup></sup>. Adeno-associated virus (AAV) is a preferred viral vector due to its lack of pathogenicity, high transduction efficiency, and long-term transgene expression<sup>e.g.,<sup>2,6,7</sup></sup>, and it is typically administered by intravitreal injection to transduce inner retinal cells (e.g., ganglion and Müller cells). Of the many AAV serotypes that have been identified, serotype 2 is the most studied in retina<sup>8,9</sup>.

Although animal models of viral mediated gene delivery to the retina are motivated by the development of gene therapy for human, the uniqueness of the human eye may make viral transduction studies in common mammalian models (e.g., rats, mice, rabbits) a poor predictor of transduction in humans. The macaque closely matches humans phylogenetically, as well as in structural features that may be important for retinal transduction, including eye size<sup>10-12</sup>, the configuration of the high-acuity fovea<sup>13</sup>, a thick nerve fiber layer (NFL)<sup>14</sup> and inner limiting membrane (ILM)<sup>15</sup> on the retinal surface. However, only a handful of studies have explored AAV2 transduction in macaque eyes by intravitreal injection (Merigan WH, et al. *IOVS* 2008;49:ARVO E-Abstract 4514)<sup>6,16</sup>, and they suggest that primate retina may have unique barriers to transduction that have not been identified in other animal models.

Here, we describe AAV2 mediated transduction of the macaque retina by intravitreal injection using green fluorescent protein (GFP) as a reporter. Because of the biological significance of human foveal vision<sup>17,18</sup>, one focus of our study was to evaluate the efficiency and selectivity of AAV2 with different promoters for transducing inner retinal cells in the fovea, which are excellent targets for retinal gene therapy. To this end, various neuronal (hCx36, hCx36sh and hSYN) and ubiquitous (CBA, smCBA) promoters were evaluated. The GFP expression driven by those promoters was tracked over time with a fundus camera optimized to

detect GFP fluorescence. When strong expression was reached, the subcellular localization of GFP expression was examined using fluorescence adaptive optics (AO) imaging<sup>e.g., 19</sup>, which provides substantially higher resolution and sensitivity than fundus imaging. These *in vivo* imaging results were then confirmed with histology. We found dense ganglion cell transduction with the hCx36 promoter in primate fovea, as well as non-selective transduction of Müller and ganglion cells with the ubiquitous CBA promoter. Moreover, our results show that transduction patterns of AAV2 in the macaque eye by intravitreal injection is qualitatively similar to that in the smaller eye of a foveated new-world primate marmoset<sup>20, 21</sup>, yet significantly different from that seen in other species, and in particular rodent models.

## ***Methods***

### **Subjects**

Eight adult macaque monkeys, each weighing approximately 6 kg, with ages ranging from 3-11 years at the time of injection (Table S1), were used. Eyes and retinas were normal in all studied monkeys, except for one monkey with a history of ganglion cell loss from a cortical infection and two monkeys given intravitreal injections of microplasmin, which produces vitreoretinal detachment (see *Supplementary Materials and Methods*). Head-posts were implanted in monkeys used for AO imaging, as previously described<sup>19</sup>. All animal procedures were conducted according to the ARVO Statement for the Use of Animals and the guidelines of the Office of Laboratory Animal Care at the University of Rochester.

### **Viral vectors**

#### *Preparation of vectors*

AAV vectors were packaged and purified by standard methods<sup>22</sup> in the Flannery laboratory at the University of California, Berkeley. Briefly, AAV was packaged by triple transfection (Lipofectamine 2000, Invitrogen, Carlsbad, CA) of transfer and helper plasmids into AAV293 cells. After harvest, lysis, and iodixanol ultracentrifugation, the interphase between the 54% and 40% iodixanol fraction, and the lower three-quarters of the 40% iodixanol fraction were extracted and further purified by heparin affinity chromatography. The eluent was concentrated and buffer exchanged using an Amicon Ultra-15 centrifugal filter unit. Virus was washed three times with fifteen milliliters of sterile phosphate buffered saline (PBS) with 0.001% Tween. Vector was then titered by quantitative PCR (QPCR) relative to standards.

#### *Promoter and gene payload of AAV2 vector*

The AAV vectors produced for this study were AAV2/2 (i.e. AAV2 inverted terminal repeat containing genomes packaged inside AAV2 capsid, termed AAV2 in this paper) carrying GFP (either the enhanced GFP (eGFP) or humanized GFP (hGFP)) transgene (see Table S1).

One of the following five promoters (Table 1) was used to drive the transgenes: chicken- $\beta$ -actin (CBA) with cytomegalovirus (CMV) enhancer, human connexin 36 (hCx36), human synapsin (hSYN), and shortened versions of CBA and hCx36 (smCBA and hCx36sh, respectively). In some cases, the transduction efficiency was evaluated by injection of 5  $\mu$ l of the same vector into wild type rat eyes. For primate injections, viral vectors were shipped on ice to University of Rochester from UC Berkeley. The viral vector was then stored at 4 °C until use, normally within 1-2 weeks. All *in vivo* imaging and post-mortem histology were carried out at University of Rochester.

The sequences of CBA and smCBA have been described previously (Boye SL, et al. *IOVS* 2006;47:ARVO E-Abstract 852)<sup>23</sup>. The sequences of hCx36 and hCx36sh have not been described previously (Greenberg K, manuscript in preparation, 2010). The 2.8 kb (hCx36) and 1.8 kb (hCx36sh) fragments of the hCx36 promoter were cloned from human genomic DNA using standard molecular biology techniques and high fidelity polymerase chain reaction. The promoter fragments were then ligated into an AAV2 backbone vector containing GFP and the WPRE. All vectors were sequenced for PCR fidelity. The sequence of hSYN has been described by Kugler et al.<sup>24,25</sup>.

#### *Intravitreal injection*

Viral vector (40 - 100  $\mu$ l) was injected into the vitreous of each eye through the sclera approximately 3mm behind the limbus, using a 30-gauge needle, with precautions to avoid infection. The condition of the injected eyes was monitored closely for up to two weeks. Three eyes from two animals were pretreated by an intravitreal injection of 50  $\mu$ g (in 100  $\mu$ l distilled water) of recombinant microplasmin (Thrombogenics, Leuven, Belgium; see Table S1), a recombinant serine protease that is used to degrade the vitreo-retinal junction and produce

posterior vitreal detachment in human eye<sup>26</sup>. These injections were given using identical procedures 5 days before the injection of viral vector.

In cases when both eyes were injected with vector, the second injection was performed less than one month after the first injection (Table S1), to avoid immune inactivation of the second injection by antibodies against AAV2 from the first injection<sup>27</sup>. Serum antibody titer against AAV2 was measured in the Schaffer laboratory at UC Berkeley (see *Supplementary Materials and Methods*). We excluded from analysis one monkey that had a high serum antibody titer against AAV2 prior to virus injection (Table S1).

### *In vivo* transduction evaluation

#### *Fundus imaging*

Color and fluorescence fundus images were taken of each studied retina using a TRC-50DX fundus camera (Topcon, Paramus, NJ). The fundus camera was modified to image GFP fluorescence, using an excitation bandpass filter of 457 nm to 487 nm (FF01-472/30; Semrock, Rochester, NY), and a barrier filters with a bandpass of 502.5 nm to 537.5 nm (FF01 520/35, Semrock, Rochester, NY). Contrast and brightness of all fundus images presented in this paper were adjusted in Photoshop (Adobe Systems, Waltham, MA) for better visualization of the relatively weak fluorescence signal of the GFP expressed in retinal neurons. Fundus images from the right eyes were flipped horizontally to match those from the left eyes, so that all fundus images presented in the paper have the same orientation. Scale bars for fundus images (Figs. 1A,B, 4A and 7) were calculated assuming that the distance between the fovea center and temporal edge of the optic disk is 11.8 degrees<sup>28</sup>.

#### *AO imaging*

The fluorescence adaptive optics scanning laser ophthalmoscope (FAOLSO) was used to image retinal neurons that expressed GFP *in vivo*, as previously described<sup>19,29</sup>. During imaging

sessions, the monkeys were anesthetized with isoflurane at a dosage (typically 2%) sufficient to minimize large ocular movements and eliminate microsaccades. Images (1500 frames, and at a field of view of 2 to 3 degrees) were acquired simultaneously in two channels: (1) a reflectance channel which captured infrared light ( $794 \pm 17$  nm) reflected from cones, and (2) a fluorescence channel which captured the fluorescence emission from GFP in retinal neurons excited by laser light at 488 nm.

To acquire through-focus images, we used a deformable mirror to focus the imaging plane through the depth of retina. To equate diopters of focus ( $F$ , in units of D) to axial distance ( $L$ , in units of  $\mu\text{m}$ ) in retina, we used the Elmsley model for an emmetropic eye<sup>19</sup>:

$$L = \frac{4}{3} \left[ \frac{1}{D_{eye} + F} - \frac{1}{D_{eye}} \right] \times 10^6,$$

where the  $D_{eye}$  is the power of the macaque eye. For the animals used in this study, a normative eye power of 74.2 D was assumed<sup>30</sup>. 0.1 D corresponds to approximately 24  $\mu\text{m}$ .

## Histology

### *Ex vivo preparation*

For animals euthanized for histological analysis (see Table S1), eyes were enucleated from the animal immediately after euthanasia and fixed by immersion in 4% paraformaldehyde (in 0.1 M phosphate buffer). Retina, with pigment epithelium attached, was separated from sclera. Retinal whole-mounts were flattened on a glass slide by making several radial cuts at the periphery, and covered by a coverslip with mounting medium (Vectorshield, Vector Laboratories, Burlingame, CA). Transverse sections were prepared from retinal tissue embedded in agar and sectioned parallel to the horizontal raphe at 60  $\mu\text{m}$  thickness on a vibratome (Microm International GmbH, Walldorf, Germany).

Some samples were processed with immunostaining to increase the sensitivity of detection of GFP in the tissue. After washing in 0.01 M PBS, and pretreatment solution (0.4% Triton X-100 in 0.01 M PBS), the retina was incubated in blocking buffer (5% normal goat serum, 0.4% Triton X-100 in 0.01 M PBS) for 4-6 hours at room temperature followed by overnight at 4 °C to reduce nonspecific binding. We reacted the retina with primary antibody, chicken anti-EGFP (Millipore Bioscience Research Reagents, Temecula, CA) at a dilution of 1:500. The reaction was carried out initially at room temperature for 2 h, then at 4° C for 3-4 days. After several washes in PBS, we reacted the retina with the secondary antibody, goat anti-chicken conjugated with Alexa 488 (Invitrogen, Carlsbad, CA), to visualize the primary antibody staining (1-2 days, in dark at 4 °C).

#### *Ex vivo confocal imaging*

*Ex vivo* whole-mount and transverse sections were imaged using a confocal microscope (Zeiss LSM 510 Meta, Carl Zeiss, Thornwood, NY). GFP fluorescence in the tissue, or Alexa 488 signal after immunostaining was imaged with settings optimized for FITC. Image stacks were obtained across z-depths for whole-mount tissue. Z-projection and transverse views of the image stacks were generated using NIH Image software (<http://rsb.info.nih.gov/nih-image/>). Brightness and contrast of the images presented in this paper were adjusted in Photoshop (Adobe Systems, Waltham, MA) for better visualization. Montages of images from adjacent retinal regions were also processed in Photoshop (Adobe Systems, Waltham, MA).

#### *Conversion between angular and retinal distances*

Since *in vivo* fundus and AO images were measured in angular distance (degrees of visual angle), and *ex vivo* confocal imaging were measured in retinal distance ( $\mu\text{m}$ ), we assume 223  $\mu\text{m}$  in retinal distance for 1 degree in angular distance<sup>31</sup>. Converted values are quoted within parenthesis.

## Results

AAV2 transduction in macaque eye occurred in fovea and peripheral retina, but not in central retina outside the fovea. Foveal transduction was more consistent across promoters than was peripheral transduction.

### AAV2-hCx36-GFP transduces foveal ganglion cells, but not Müller cells.

Intravitreal injection of AAV2-hCx36-GFP resulted in a dense annulus of GFP expression around the fovea, clearly visible *in vivo*, as evaluated with either fundus or adaptive optics (AO) imaging (Fig. 1; four eyes were tested, see Table S1). The inner edge of this annulus was approximately 1.5 degrees ( $\sim 0.3$  mm) from the foveal center, which closely matches the location of the outer edge of the foveal avascular zone<sup>32</sup> (Fig. 1A,B). The outer edge of the annulus was approximately 2.5 degrees ( $\sim 0.6$  mm) from the fovea center. GFP-expressing axon bundles projecting from the annular ring formed an arcuate pattern converging on the temporal side of the optic disc (Fig. 1B)<sup>33</sup>. Individual GFP-expressing cell bodies are visible in AO images (Fig. 1C). The density of transduced cells dropped gradually over about 100  $\mu\text{m}$  from GFP expression in many retinal cells at the outer edge of the annulus, to expression below the detection limit (Fig. 1C; and see also Fig. 2C,D). The first appearance of the transduction illustrated in these data was rapid, with the fluorescence signal of GFP first visible by fundus camera less than 1.5 months after injection for the eye shown in Figure 1A, and the expression has remained stable for more than 2.5 years after vector injection.

Through-focus AO images of the GFP expressing annulus showed a complete lack of GFP expression in Müller cells with the neuronal hCx36 promoter (Fig. 1D,E). GFP-expressing cells in the inner portion of the annulus are in sharp view at deep focus (arrows in Fig. 1D), but not at the superficial focus (arrows in Fig. 1E), while GFP-expressing cells in the outer portion of

the annulus are in sharp view at the superficial focus (arrowheads in Fig. 1E), but not at the deep focus (arrowheads in Fig. 1D). The deep focus image (Fig. 1D) shows a few scattered cells within the foveal avascular zone (open triangle), which may be ganglion cells, as described by Grünert et al.<sup>34</sup>.

*Ex vivo* confocal images of retinal whole-mounts confirmed AAV2-hCx36-GFP transduction in foveal cells in the ganglion cell layer (GCL), but did not involve Müller cells. Because ganglion cells comprise 95% of the neuronal cell population in the GCL in fovea (displaced amacrine cells are 5% or less<sup>35,36</sup> (see also Curcio and Allen<sup>13</sup> for human retina), most of the GFP-expressing cells are ganglion cells. The inner edge of the GFP-expression annulus showed no expression of GFP in Müller cells below the ganglion cell layer (Fig. 2B), confirming the *in vivo* observation (Fig. 1D,E). The outer edge of the GFP-expression annulus also showed no intervening Müller cell processes between the individual cell somas in the ganglion cell layer (Fig. 2C,D). GFP-expression was also visible in the inner plexiform layer (IPL), where the dendrites of transduced ganglion cells extend (Fig. 2B). We also observed scattered GFP-expressing cell somas in the inner nuclear layer (INL), close to the IPL/INL border, which could be amacrine cells<sup>37</sup> (data not shown).

While AAV2-hCx36-GFP produced strong foveal transduction in normal eyes, no retinal transduction was seen in central retina outside the annulus of foveal GFP (data not shown). In peripheral retina, we observed scattered transduction of cells in the GCL, especially along blood vessels (data not shown). GFP expression was also found in peripheral retina in eyes that received enzymatic vitreolysis with microplasmin prior to vector injection (see *Methods*, and Table S1). For the eye shown in Figure 3, GFP expression was visible in Müller cells and retinal cells in both GCL and INL at the distal edge of far nasal peripheral retina extending

approximately 2 mm (~ 9 degrees) toward central retina. This peripheral transduction was visible in fundus images as dense GFP-expressing axons entering the optic disc from nasal retina (data not shown).

### AAV2-CBA-GFP transduced both ganglion cells and Müller cells in fovea and peripheral retina

Intravitreal injection of AAV2-CBA-GFP resulted in a disc of GFP expression centered on the fovea and extending to more than 1.5 degrees (~ 0.3 mm) eccentricity, which was clearly visible *in vivo*, as evaluated by fundus and AO images (Fig. 4A-C; one eye was tested, see Table S1). GFP expression in axon bundles appeared less intense with the CBA promoter than with the hCx36 promoter and could barely be seen in the fundus image (Fig. 4A compared to Fig. 1B). However, GFP-expressing axon bundles, as well as individual retinal cells, were clearly seen in AO images (Fig. 4B,C). GFP expression produced by AAV2-CBA-GFP took much longer to develop than AAV2-hCx36-GFP, with no funduscopically visible transduction even at 4 months after viral injection, and the next examination at 10 months showed stable expression. However, the lower titer of the AAV2-CBA-GFP relative to the AAV2-hCx36-GFP precludes comparison of transduction efficiency of CBA and hCx36 promoters (see Table S1).

Through-focus AO images showed that foveal Müller cells are densely transduced. The three dimensional morphology of the GFP-expressing Müller cells and distribution of ganglion cells in the foveal region can be seen through a series of AO images across retinal depths from outer retina towards inner retina (Fig. 4D-G). In Figure 4D, Müller cell processes at the outer retina are in focus, while in Figure 4G, more superficial ganglion cell somas are in focus. The lateral displaced processes of the Müller cells, and their soma are best visualized in the intermediate focuses (respectively Fig. 4E,F). These GFP-expressing Müller cells are responsible for the solid, disk-like appearance of the GFP expression in the fundus image (Fig. 4A).

*Ex vivo* confocal images confirm that AAV2-CBA-GFP transduces both foveal ganglion cells and Müller cells (Fig. 5). As shown in the transverse section through the GFP-expressing disc centered on the fovea (Fig. 5B), GFP-expressing Müller cells extend their processes throughout the full thickness of the retina, with the sclerad end of their processes terminating near the outer limiting membrane (OLM) and the vitread end of their processes terminating at the ILM<sup>38</sup>. The lateral displacement between the sclerad and vitread ends of Müller cell processes reflect the underlying anatomy: Müller cells ensheath cones in the fovea center that provide inputs to ganglion cells that are displaced away from the fovea center<sup>39</sup>. GFP-expressing ganglion cells extended to slightly greater eccentricity than Müller cells (Fig. 5B). Most GFP expressing cell somas in the INL appeared to be Müller cells (Fig. 5B).

Transduction of peripheral retina by AAV2-CBA-GFP was evident in the *ex vivo* confocal images. The density of GFP-expressing retinal cells gradually increased from an eccentricity of approximately 8 mm (~ 30 degrees) from the fovea center (data not shown) to the edge of the retina (Fig. 6A). Density of GFP-expressing retinal cells at the far peripheral retina was relatively sparse compared to that seen immediately around the fovea center (Fig. 6A compared to Fig. 5). As illustrated by the example shown in Figure 6B-D from one far peripheral location, the majority of GFP-expressing cells were Müller cells, and transduction in ganglion cells was less pronounced, such that the axons of these ganglion cells could not be seen in fundus images (data not shown).

Shorter promoters were ineffective in normal retinas, but produced transduction in retinas with ganglion cell loss, or enzymatic vitreolysis.

Since AAV vectors have a limited packaging capacity, we explored the use of shorter neuronal and ubiquitous promoters to drive GFP expression in the primate retina.

We examined transduction by two short neuronal promoters - hSYN<sup>24</sup> and the shortened hCx36 promoter (hCx36sh) - in normal and diseased eyes with ganglion cell loss (one eye for each condition; see Table S1 and Fig. S1), and compared both to transduction with hCx36 promoter. As shown by fundus images (Fig. 7A,C), intravitreal injection of AAV2 with neither promoter produced visible GFP expression in normal retinas over durations that exceeded the time needed for transduction by hCx36, but in both cases (at comparable titer; see Table S1) produced visible GFP expression (Fig. 7B,D) in eyes with loss of ganglion cells (see Fig. S1A). However, the lower titers of the AAV2-hSYN-GFP and AAV2-hCx36sh-GFP than the AAV2-hCx36-GFP preclude comparison of transduction efficiency of the two short neuronal promoters to hCx36 promoter (see Table S1).

We also examined the transduction by the short CBA promoter (smCBA) in a normal eye and an eye that received enzymatic vitreolysis with microplasmin (see *Methods*) prior to vector injection (one eye for each condition; see Table S1), and compared both to the transduction with CBA promoter (at comparable titer; see Table S1). As shown by fundus images (Fig. 7E,F), intravitreal injection of AAV2-smCBA-GFP produced no visible GFP expression in normal retina (Fig. 7E) over a duration that exceeded the time needed to produce expression with the full-length CBA promoter, but produced visible GFP expression in the eye pre-treated with microplasmin (Fig. 7F). For the latter, the appearance of foveal transduction (Fig. 7F) was similar to that of the full-length CBA promoter (Fig. 4A), and we confirmed by histology that both foveal ganglion cells and Müller cells were transduced (data not shown). Besides foveal transduction, prominent transduction in far peripheral ganglion cells was also visible in the fundus image (Fig. 7F) as dense GFP expression in axons entering the optic disc from nasal

retina, and we verified by histology that both Müller cells and ganglion cells at the distal edge of far peripheral retina are transduced (data not shown).

## ***Discussion***

This study found that intravitreal injection of AAV2 into the macaque eye produced dense ganglion cell and Müller cell transduction only in a narrow region surrounding the fovea, with no transduction in central retina beyond the fovea and little or no transduction in peripheral retina. This result differs from the more uniform transduction reported after intravitreal injection in other species, including rodents <sup>e.g., 8, 40</sup>, and raises the question of how well studies in non-primates are predictive of gene therapy results in humans.

### What limits transduction of macaque inner retina?

The limited transduction we observed may be due to the physical barriers posed by the anatomy of the macaque retina, such as the nerve fiber layer (NFL) and inner limiting membrane (ILM) which lie along the surface of the retina, between ganglion cell layer and vitreous.

Thickness variation of the NFL across the retina is consistent with the transduction patterns observed in this study. There is a complete absence of nerve fiber layer covering the foveal retinal location where inner retinal cells were transduced (see Figs. 1B and 4A). Outside the fovea, superior and inferior to the optic disc, NFL thickness can reach a maximal thickness of more than 200  $\mu\text{m}$  in macaque retina, and over 300  $\mu\text{m}$  in human retina <sup>14</sup>. These are the regions where no transduction was observed. When nerve fiber layer thickness was greatly reduced in retinas with ganglion cell loss, inner retina transduction was enhanced (Fig. 7B,D; see Fig. S1). A similar phenomenon has been reported in degenerated rodent retina <sup>41</sup>. Together these results suggest enhanced transduction in the disease compromised retina, an advantage from the gene delivery perspective.

Although the ILM is thin compared to the NFL, its thickness is inversely related to the inner retina transduction efficiency observed in this study. Macaque (and human) ILM is thinnest in the fovea, where transduction is best, moderately thicker in the far peripheral retina, where

expression was modest, and thickest in posterior retina near the fovea, where almost no transduction was observed<sup>15</sup>. Furthermore, the ILM is thinner above retinal vessels<sup>15</sup>, where we observed focal transduction of retinal cells along blood vessels at eccentricities beyond about 30 degrees (data not shown). Microplasmin, which disrupts the border between vitreous and ILM, increased transduction by AAV2-hCx36 and AAV2-smCBA in far peripheral retina where the ILM is relatively thin, similar to the increased transduction in rodent when the ILM was disrupted by a protease<sup>42</sup>. The human and macaque ILM are very similar<sup>15</sup>, and thus the inner limiting membrane will most likely be a barrier to AAV mediated gene delivery in humans.

The pattern of foveal transduction could also reflect other features of the primate retina that interact with AAV2 capsids, such as the distribution of cell surface receptors, since AAV2 binds selectively to heparin sulfate proteoglycan, and three co-receptors<sup>43-47</sup>. The topographical distribution of these receptors has not been measured in macaque retina. However, the dense transduction at the fovea indicates that promoter selectivity is not the basis for a lack of transduction in other areas of retina.

### Which animal models are optimal for developing human gene therapy?

The wide variety of animal models used in gene therapy research each fills an important role. Rodents (e.g., mice) are widely used species well suited for genetic manipulations, whereas dogs and cats provide several unique models of retinal degeneration and greater similarity to human retina due to the large eye size and higher acuity area centralis. The non-human primate is better suited than the above species for predicting transduction in humans because of the unique morphology of the retina in species that have a fovea.

Recently, transduction of inner retina by intravitreal injection was studied in one non-human primate, the New World marmoset<sup>20</sup>, using an AAV2 virus with either the CAG (hybrid

CMV early enhancer/chicken  $\beta$ -actin) or CMV (human cytomegalovirus immediate-early gene) promoter<sup>21</sup>. The marmoset has a small eye, with an average axial length of 11 mm<sup>48</sup>, substantially smaller than that of macaque (18 mm)<sup>49</sup> and human (24 mm)<sup>50</sup>. Marmosets have a well-developed fovea, similar to that of macaque and human<sup>51</sup> in both overall shape and the extent of ganglion cell displacement away from the foveal center.

However, the transduction of marmoset retina observed by Ivanova et al.<sup>21</sup> was quite different from that observed in the macaque in our laboratory in three respects: cellular selectivity, the spatial pattern of transduction across the retina, and the depth of transduction through the retina. The CBA promoter used in the present study and the CAG promoter used in the marmoset study of Ivanova et al.<sup>21</sup> are similar<sup>23</sup>. Despite this similarity, the macaque showed Müller cell and ganglion cell transduction at the fovea and largely Müller cell transduction in peripheral retina, while the marmoset showed no Müller cell transduction at any retinal location, but substantial ganglion cell transduction across the retina. The spatial pattern of transduction across the retina was also different, with the macaque showing dense GFP expression in foveal ganglion cells, but little GFP-expression in peripheral ganglion cells, while marmoset showed relatively sparse foveal ganglion cell transduction, but substantial peripheral ganglion cell transduction. Finally the depth of transduction through the retina also differed between macaque and marmoset. Neuronal transduction in the macaque retina was confined to the GCL and inner portion of the INL, whereas the transduction in marmoset extends to outer retina (e.g., photoreceptors).

We speculate that these differences between macaque and marmoset could be due to both species differences in viral tropism and a difference in the topology of a physical barrier, such as the ILM, which has not been studied in marmoset. Given that macaque is closer to human in

evolutionary lineage<sup>52</sup>, and the great similarity in physical attributes of the two species, such as eye size<sup>53</sup> and ILM thickness<sup>15</sup>, it is likely that the transduction observed in macaques in this study provides a closer prediction of transduction by intravitreal injection in humans than that observed in marmoset. However, further research is needed to address this issue, due to differences in promoter, age, and viral titer between the studies in the two species.

### Choice of vector and promoter for transducing macaque inner retina

AAV2, with the hCx36 promoter, produced, selective transduction of foveal ganglion cells, but not Müller cells, making it a good choice to insert gene products into ganglion cells for neurophysiology studies or ganglion cell neuroprotection in diseases such as glaucoma. However, the hCx36 promoter fragment used in this study is large (2.8 kb) and it occupies much of the 4.7 kb genomic capacity of AAV2<sup>54</sup>, leaving little space for transgenes substantially larger than GFP (0.7 kb). The CBA promoter (1.7 kb) is smaller than hCx36, and produces good transduction of both foveal and peripheral ganglion cells and Müller cells. The major drawback of the CBA promoter was the extended time required for expression,

The short promoters - hSYN, hCx36sh, and smCBA - did not produce visible transduction in healthy retina over an extended time and thus are not effective choices for use in macaques. Although the smCBA promoter yielded similar expression to full-length CBA when injected into an eye pre-treated with microplasmin, the hCx36sh and hSYN promoters remained ineffective even when injected into eyes altered by ganglion cell loss. The fact that the AAV2 vectors with two of these promoters (smCBA and hSYN) have produced excellent retinal transduction in other mammals (Boye SL, et al. *IOVS* 2006;47:ARVO E-Abstract 852)<sup>e.g., 7, 42, 55</sup> illustrates the unique difficulty in achieving gene expression in the primate retina.

### The importance of *in vivo*, high-resolution AO imaging to monitor viral transduction in macaque

Although histological verification remains the standard method for evaluating the efficiency and selectivity of transduction by viral vectors, *in vivo* imaging is particularly important in investigating therapeutic effects of gene therapy in primates, as it can eliminate the need to serially sacrifice different animals for post-mortem histology. Fundus imaging can reveal the time course and spatial pattern of expression in each animal. Because AO imaging has substantially greater sensitivity and spatial resolution than fundus imaging, as well as axial sectioning capacity (through-focus; see Fig. 1D,E and Fig. 4D-G), it is able to reveal details of GFP expression that could not be determined from the fundus images. This distinction was particularly evident in this study when visualizing ganglion cell transduction by CBA, which was clear in AO images (Fig. 4B-G), but barely observable in fundus image (Fig. 4A).

### Implications of this study for human retinal gene therapy

A significant issue in moving viral-mediated gene therapies for human retinal disease from small animal efficacy studies to clinical applications are potential differences between the eye and retina of the animal model and human (e.g., retinal cell-surface properties, promoter selectivity and anatomy of the retina). Studies in the ideal animal model, the macaque monkey, are severely limited by availability cost, and lack of appropriate disease models, but need to be carried out to develop successful retinal gene therapy for humans. This study demonstrates that barriers to transduction of inner retina in macaque are substantial, but also shows that the use of high-resolution, *in vivo* adaptive optics imaging greatly facilitates such investigation.

***Acknowledgements***

This work was supported by a grant from Bausch and Lomb, Inc.; NIH research grants EY019375, BRP-EY014375, R01-HL081527, and NDC 5PN2EY018241; NIH Training Grant-EY07125; NIH Core Grant-EY001319; NSF Science and Technology Center for Adaptive Optics (Santa Cruz, CA, managed by the University of California at Santa Cruz, cooperative agreement no.: AST-9876783) and Grants from the Foundation Fighting Blindness and Research to Prevent Blindness. We thank Jennifer Strazzeri (Flaum Eye Institute, University of Rochester) for technical assistance, surgery and fundus photography, and Thurma McDaniel and Tracey Bubel (Center for Visual Science, University of Rochester) for assistance with histology. Commercial relationships: David R. Williams, Bausch and Lomb (F, C), Optos (C), Adaptive Optics (P); William H. Merigan, Bausch and Lomb (F).

## References

1. Harvey AR, Hu Y, Leaver SG, et al. Gene therapy and transplantation in CNS repair: the visual system. *Prog Retin Eye Res* 2006;25:449-489.
2. Daya S, Berns KI. Gene therapy using adeno-associated virus vectors. *Clin Microbiol Rev* 2008;21:583-593.
3. Mancuso K, Hauswirth WW, Li Q, et al. Gene therapy for red-green colour blindness in adult primates. *Nature* 2009;461:784-787.
4. Tan MH, Smith AJ, Pawlyk B, et al. Gene therapy for retinitis pigmentosa and Leber congenital amaurosis caused by defects in AIP1: effective rescue of mouse models of partial and complete Aip1 deficiency using AAV2/2 and AAV2/8 vectors. *Hum Mol Genet* 2009;18:2099-2114.
5. Maguire AM, High KA, Auricchio A, et al. Age-dependent effects of RPE65 gene therapy for Leber's congenital amaurosis: a phase 1 dose-escalation trial. *Lancet* 2009;374:1597-1605.
6. Leberherz C, Auricchio A, Maguire AM, et al. Long-term inducible gene expression in the eye via adeno-associated virus gene transfer in nonhuman primates. *Hum Gene Ther* 2005;16:178-186.
7. Petrs-Silva H, Dinculescu A, Li Q, et al. High-efficiency transduction of the mouse retina by tyrosine-mutant AAV serotype vectors. *Mol Ther* 2009;17:463-471.
8. Hellstrom M, Ruitenberg MJ, Pollett MA, et al. Cellular tropism and transduction properties of seven adeno-associated viral vector serotypes in adult retina after intravitreal injection. *Gene Ther* 2009;16:521-532.
9. Surace EM, Auricchio A. Versatility of AAV vectors for retinal gene transfer. *Vision Res* 2008;48:353-359.
10. Rolling F. Recombinant AAV-mediated gene transfer to the retina: gene therapy perspectives. *Gene Ther* 2004;11 Suppl 1:S26-32.
11. Buch PK, Bainbridge JW, Ali RR. AAV-mediated gene therapy for retinal disorders: from mouse to man. *Gene Ther* 2008;15:849-857.
12. Stieger K, Lheriteau E, Moullier P, Rolling F. AAV-mediated gene therapy for retinal disorders in large animal models. *ILAR J* 2009;50:206-224.
13. Curcio CA, Allen KA. Topography of ganglion cells in human retina. *J Comp Neurol* 1990;300:5-25.
14. Frenkel S, Morgan JE, Blumenthal EZ. Histological measurement of retinal nerve fibre layer thickness. *Eye (Lond)* 2005;19:491-498.
15. Matsumoto B, Blanks JC, Ryan SJ. Topographic variations in the rabbit and primate internal limiting membrane. *Invest Ophthalmol Vis Sci* 1984;25:71-82.
16. Leberherz C, Maguire AM, Auricchio A, et al. Nonhuman primate models for diabetic ocular neovascularization using AAV2-mediated overexpression of vascular endothelial growth factor. *Diabetes* 2005;54:1141-1149.
17. Cheung SH, Legge GE. Functional and cortical adaptations to central vision loss. *Vis Neurosci* 2005;22:187-201.

18. Harrison ER. Visual acuity and the cone cell distribution of the retina. *Br J Ophthalmol* 1953;37:538-542.
19. Gray DC, Wolfe R, Gee BP, et al. In vivo imaging of the fine structure of rhodamine-labeled macaque retinal ganglion cells. *Invest Ophthalmol Vis Sci* 2008;49:467-473.
20. Troilo D, Howland HC, Judge SJ. Visual optics and retinal cone topography in the common marmoset (*Callithrix jacchus*). *Vision Res* 1993;33:1301-1310.
21. Ivanova E, Hwang GS, Pan ZH, Troilo D. Evaluation of AAV-Mediated Expression of Chop2-GFP in the Marmoset Retina. *Invest Ophthalmol Vis Sci* 2010.
22. Zolotukhin S, Byrne BJ, Mason E, et al. Recombinant adeno-associated virus purification using novel methods improves infectious titer and yield. *Gene Ther* 1999;6:973-985.
23. Fitzsimons HL, Bland RJ, During MJ. Promoters and regulatory elements that improve adeno-associated virus transgene expression in the brain. *Methods* 2002;28:227-236.
24. Kugler S, Lingor P, Scholl U, Zolotukhin S, Bahr M. Differential transgene expression in brain cells in vivo and in vitro from AAV-2 vectors with small transcriptional control units. *Virology* 2003;311:89-95.
25. Kugler S, Kilic E, Bahr M. Human synapsin 1 gene promoter confers highly neuron-specific long-term transgene expression from an adenoviral vector in the adult rat brain depending on the transduced area. *Gene Ther* 2003;10:337-347.
26. Gandorfer A, Rohleder M, Sethi C, et al. Posterior vitreous detachment induced by microplasmin. *Invest Ophthalmol Vis Sci* 2004;45:641-647.
27. Li Q, Miller R, Han PY, et al. Intraocular route of AAV2 vector administration defines humoral immune response and therapeutic potential. *Mol Vis* 2008;14:1760-1769.
28. Kolb H, Fernandez E, Nelson R. Facts and Figures Concerning the Human Retina. In: Kolb H, Fernandez E, Nelson R (eds), *Webvision: The Organization of the Retina and Visual System*. Salt Lake City: University of Utah, John Moran Eye Center; 2007.
29. Gray DC, Merigan W, Wolfing JI, et al. In vivo fluorescence imaging of primate retinal ganglion cells and retinal pigment epithelial cells. *Opt Express* 2006;14:7144-7158.
30. Lapuerta P, Schein SJ. A four-surface schematic eye of macaque monkey obtained by an optical method. *Vision Res* 1995;35:2245-2254.
31. Perry VH, Cowey A. The ganglion cell and cone distributions in the monkey's retina: implications for central magnification factors. *Vision Res* 1985;25:1795-1810.
32. Snodderly DM, Weinhaus RS, Choi JC. Neural-vascular relationships in central retina of macaque monkeys (*Macaca fascicularis*). *J Neurosci* 1992;12:1169-1193.
33. Ogden TE. Nerve fiber layer of the macaque retina: retinotopic organization. *Invest Ophthalmol Vis Sci* 1983;24:85-98.
34. Grünert U, Greferath U, Boycott BB, Wassle H. Parasol (P alpha) ganglion-cells of the primate fovea: immunocytochemical staining with antibodies against GABAA-receptors. *Vision Res* 1993;33:1-14.
35. Wassle H, Grünert U, Rohrenbeck J, Boycott BB. Cortical magnification factor and the ganglion cell density of the primate retina. *Nature* 1989;341:643-646.
36. Wassle H, Grünert U, Rohrenbeck J, Boycott BB. Retinal ganglion cell density and cortical magnification factor in the primate. *Vision Res* 1990;30:1897-1911.

37. Ahmad KM, Klug K, Herr S, Sterling P, Schein S. Cell density ratios in a foveal patch in macaque retina. *Vis Neurosci* 2003;20:189-209.
38. Distler C, Dreher Z. Glia cells of the monkey retina--II. Müller cells. *Vision Res* 1996;36:2381-2394.
39. Schein SJ. Anatomy of macaque fovea and spatial densities of neurons in foveal representation. *J Comp Neurol* 1988;269:479-505.
40. Ali RR, Reichel MB, De Alwis M, et al. Adeno-associated virus gene transfer to mouse retina. *Hum Gene Ther* 1998;9:81-86.
41. Kolstad KD, Dalkara D, Guerin K, et al. Changes in adeno-associated virus-mediated gene delivery in retinal degeneration. *Hum Gene Ther* 2010;21:571-578.
42. Dalkara D, Kolstad KD, Caporale N, et al. Inner limiting membrane barriers to AAV-mediated retinal transduction from the vitreous. *Mol Ther* 2009;17:2096-2102.
43. Summerford C, Samulski RJ. Membrane-associated heparan sulfate proteoglycan is a receptor for adeno-associated virus type 2 virions. *J Virol* 1998;72:1438-1445.
44. Summerford C, Bartlett JS, Samulski RJ. AlphaVbeta5 integrin: a co-receptor for adeno-associated virus type 2 infection. *Nat Med* 1999;5:78-82.
45. Bartlett JS, Wilcher R, Samulski RJ. Infectious entry pathway of adeno-associated virus and adeno-associated virus vectors. *J Virol* 2000;74:2777-2785.
46. Bartlett JS, Samulski RJ, McCown TJ. Selective and rapid uptake of adeno-associated virus type 2 in brain. *Hum Gene Ther* 1998;9:1181-1186.
47. Qing K, Mah C, Hansen J, Zhou S, Dwarki V, Srivastava A. Human fibroblast growth factor receptor 1 is a co-receptor for infection by adeno-associated virus 2. *Nat Med* 1999;5:71-77.
48. Troilo D, Nickla DL. The response to visual form deprivation differs with age in marmosets. *Invest Ophthalmol Vis Sci* 2005;46:1873-1881.
49. Qiao-Grider Y, Hung LF, Kee CS, Ramamirtham R, Smith EL, 3rd. Recovery from form-deprivation myopia in rhesus monkeys. *Invest Ophthalmol Vis Sci* 2004;45:3361-3372.
50. Kubo E, Kumamoto Y, Tsuzuki S, Akagi Y. Axial length, myopia, and the severity of lens opacity at the time of cataract surgery. *Arch Ophthalmol* 2006;124:1586-1590.
51. Hendrickson AE. Organization of the Adult Primate Fovea. In: Penfold PL, Provis JM (eds), *Macular Degeneration*. Berlin Heidelberg New York: Springer; 2005:1-23.
52. Lewin R. *Human evolution: an illustrated introduction*. 5th ed. Oxford, UK: Blackwell Publishing Ltd; 2005.
53. Qiao-Grider Y, Hung LF, Kee CS, Ramamirtham R, Smith EL, 3rd. Normal ocular development in young rhesus monkeys (*Macaca mulatta*). *Vision Res* 2007;47:1424-1444.
54. Dong JY, Fan PD, Frizzell RA. Quantitative analysis of the packaging capacity of recombinant adeno-associated virus. *Hum Gene Ther* 1996;7:2101-2112.
55. Geng Y, Greenberg KP, Wolfe R, et al. In vivo imaging of microscopic structures in the rat retina. *Invest Ophthalmol Vis Sci* 2009;50:5872-5879.

**Tables****Table 1.** Tested promoters

<b>Promoter</b>	<b>Abbrev.</b>	<b>Size</b>	<b>Reference</b>
Chicken- $\beta$ -actin promoter with cytomegalovirus enhancer	CBA	1.7 kb	(Boye SL, et al. <i>IOVS</i> 2006;47:ARVO E-Abstract 852) and Fitzsimons et al. <sup>23</sup>
Shortened CBA promoter	smCBA	0.95 kb	{Boye SL, et al. <i>IOVS</i> 2006;47:ARVO E-Abstract 852)
Human connexin 36 promoter	hCx36	2.8 kb	Greenberg K, manuscript in preparation, 2010
Shortened hCx36 promoter	hCx36sh	1.8 kb	
Human synapsin 1 gene promoter	hSYN	0.5 kb	Kugler et al. <sup>24, 25</sup>

## Figure Legends

**Figure 1.** *In vivo* imaging of AAV2-hCx36-GFP transduction in the macaque central retina, showing GFP expression in ganglion cells.

*A.* Fluorescence fundus image of GFP expression from AAV2-hCx36-GFP transduction (the smaller green image) superimposed on a fluorescein angiogram of central retina (the larger grey image) of the same eye. Vasculature is grey in the fluorescein angiogram. The overlay shows the relationship of the GFP expression pattern, the green annulus, to the avascular zone in the fovea.

*B.* The same fluorescence fundus image in *A* enlarged. GFP expression is visible as an annulus around the fovea, and in the bundles of labeled axons coursing from the foveal region to the optic disc. The optic disc is slightly brighter than the background, and can be seen in this image, which is not from GFP expression, but the autofluorescence of the sclera.

*C.* AO image of a portion of retina illustrated by the white dashed rectangle in *B*. Axon bundles from transduced ganglion cell coursing towards the optic disc are visible.

*D* and *E.* AO image montages at two depths of focus of the dark dashed rectangle in *B*, covering the center and temporal side of the annulus. *D* and *E* show respectively deep and more superficial focuses. Arrows mark examples of transduced cell somas within the GFP-expressing annulus that are in-focus in *D*, but out-of-focus in *E*, while arrowheads mark examples of ganglion cell somas within the annulus that are out-of-focus in *D*, but in-focus in *E*. Transduced cell somas that are in sharp focus in *E* are more peripheral than those that are in sharp focus in *D*, and thus are located farther up the foveal slope. In *D*, a few scattered cells occupying the center of the macaque fovea (see open triangle for one example) are also visible. The difference in focus between *D* and *E* corresponds to a retinal depth of 48  $\mu\text{m}$  (see *Methods*).

**Figure 2.** *Ex vivo* (histological) evaluation of AAV2-hCx36-GFP transduction in the macaque central retina, showing dense GFP expression within the ganglion cell layer in fovea.

*A.* Schematic diagram of the foveal GFP expression illustrating the location of the images in *B-D*, which are from an eye transduced with AAV2-hCx36-GFP after treatment with microplasmin (see *Methods*). Images in *B-D* show GFP expression within the ganglion cells and their axons, not amplified with immunostaining.

*B.* Confocal images of the interior edge of the annulus of GFP expression in whole-mount view (*top*) and transverse view (*bottom*) reconstructed from the portion of the whole-mount image stack between the two dashed horizontal lines. Multiple layers of transduced ganglion cells at retinal locations away from the foveal slope are visible, as well as the IPL. Numerical aperture (NA) = 1.2.

*C.* Confocal image of the superior edge of the annulus of GFP expression showing densely expressing ganglion cells and their axons. NA = 0.8.

*D.* Higher magnification image that partially overlaps with the portion of *C* marked by the rectangle. NA = 1.2.

**Figure 3.** AAV2-hCx36-GFP transduction in far peripheral retina after treatment with microplasmin.

*A-B.* GFP expression in ganglion cells (see arrowheads for examples) and Müller cells (see arrows for examples) from the nasal edge of the retina near the ora serrata. In the fluorescence fundus image of this eye, axon bundles from transduced ganglion cells were visible in the nerve fiber layer entering the optic disc from the nasal side (data not shown). In *B*, the transverse view (*right*) was reconstructed from the portion of whole-mount (*left*) image stack between the two dashed vertical lines. Transverse view shows the processes of the Müller cell

(arrow) extending towards the outer retina. GFP expression was not amplified with immunostaining. NA = 1.2.

**Figure 4.** *In vivo* images of AAV2-CBA-GFP transduction in macaque central retina, showing GFP expression in both ganglion cells and Müller cells.

*A.* Fluorescence fundus image of GFP expression. A disc of GFP expression in Müller cells is centered on the fovea, with little GFP expression evident in axon bundles originating from the fovea.

*B.* AO image of a portion of retina illustrated by the white dashed rectangle in *A*. Axon bundles from transduced ganglion cells can be seen. The two cells labeled with arrows can be used as landmarks to visualize the relative alignment of *C* and Figure 5*A*.

*C.* Higher magnification AO image of the region marked in *B* by the white dashed rectangle. At the edge of the disc of GFP expression, individual transduced retinal cells can be seen. One of the two cells from *B* is marked by an arrowhead.

*D-G.* Successive AO images of the center of the fovea (the dark dashed rectangle in *A*) at four depths of focus, illustrating the variation in retinal structure. The deepest focus in *D* shows the most central processes of the Müller cell. The most superficial focus in *G* shows the foveal Müller cell processes out of focus and the more superficial ganglion cells in focus. *E* and *F* show the intermediate focus steps, where the processes of Müller cells gradually extend from outer retina towards inner retina. A few Müller cell somas are labeled with arrows in *E* and *F*. The focus step of 0.15 D corresponds to a retinal depth of 36  $\mu\text{m}$ .

**Figure 5.** *Ex vivo* (histological) evaluation of AAV2-CBA-GFP transduction in the macaque central retina.

*A.* Confocal image of the retinal region illustrated in Figure 4*B* by the red dashed rectangle. The two retinal cells marked by arrowheads are the same cells marked by arrowheads in Figure 4*B*.

*B.* Confocal images of transverse section through the center of the fovea, illustrating GFP expression in ganglion cell somas in the ganglion cell layer (GCL) surrounding the fovea and Müller cell processes extending from outer retina to inner retina. The images from left to right overlap, but differ slightly in focal plane. The sclerad end of the processes of GFP-expressing Müller cells are located close to the foveal center (deep), and gradually course away from the fovea center towards their vitread end in the ILM above the ganglion cell layer. The thickness of the sections was 70  $\mu\text{m}$ . Examples of Müller cell somas are marked by arrows. In *A* and *B*, GFP expression was amplified with immunostaining, and NA = 0.8.

**Figure 6.** *Ex vivo* (histological) images of AAV2-CBA-GFP transduced peripheral Müller cells and ganglion cells.

*A.* Montage of confocal images of a strip of peripheral retina extending from the ora serrata approximately 5.2 mm ( $\sim 23$  degrees) towards the central retina, showing GFP expression in both scattered cells and clusters of cells. The density of transduced retinal cells declined towards central retina (direction of arrow). NA = 0.16.

*B-D.* Through focus at higher magnification of the area marked by the rectangle in *A*, showing GFP-expressing ganglion cells and Müller cells. Most transduced cells are Müller cells, shown as the dense GFP-expressing processes at the retinal surface (*B*), and sclerad end of the processes (*D*; about 43  $\mu\text{m}$  deeper than *B*) in outer retina. Arrow in *C* (about 11  $\mu\text{m}$  deeper than *B*) shows a ganglion cell. In *A-D*, GFP expression was amplified with immunostaining, and NA = 1.2.

**Figure 7.** Fundus images illustrating three shorter promoters used with AAV2 that resulted in little or no visible GFP expression in normal retinas (*A*, *C*, and *E*), but visible GFP expression in eyes with altered retinas (*B*, *D*, and *F*).

*A* and *B*. Neuronal promoter, hSYN, produced no visible GFP expression after 4.5 months (*A*), but when injected into an eye with ganglion cell loss (*B*) an annulus of GFP expression was seen in less than 2 months (data not shown; instead a later fundus image after 11 month is shown for better image quality). The transduction pattern in *B* was similar to that shown in Figure 1*A*, but the intensity of GFP expression was lower.

*C* and *D*. Shortened human connexin 36 promoter (hCx36sh) resulted in no visible GFP expression after 4.5 months (*C*; for comparison, less than 2 months was typically needed for transduction by the full-length hCx36 promoter). However, when injected into an eye with ganglion cell loss (*D*), a faint annulus of GFP expression around the fovea center was visible less than 3.5 months when the first fundus image was acquired (data not shown; instead a later fundus image after 4.5 months was shown for better image quality.) The transduction pattern in *D* was similar that shown in Figure 1*A*, but the intensity of GFP expression was lower.

*E* and *F*. Shortened CBA promoter (smCBA) resulted in no GFP expression after 15 months when injected into normal retina (*E*; for comparison, less than 10 months was needed for transduction by full-length CBA promoter). However, when injected into an eye that received enzymatic vitreolysis with microplasmin (*F*), GFP expression in fovea was visible in less than 4.5 months when the first fundus image was acquired (data not shown; instead a later fundus image after 10 months was shown for better image quality). The transduction pattern in *F* was similar to that shown in Figure 4*A*.

Figure 1

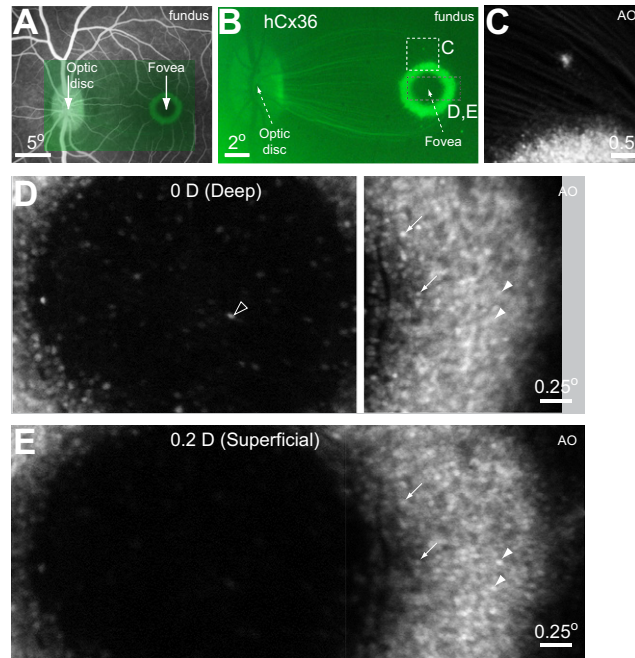


Figure 2

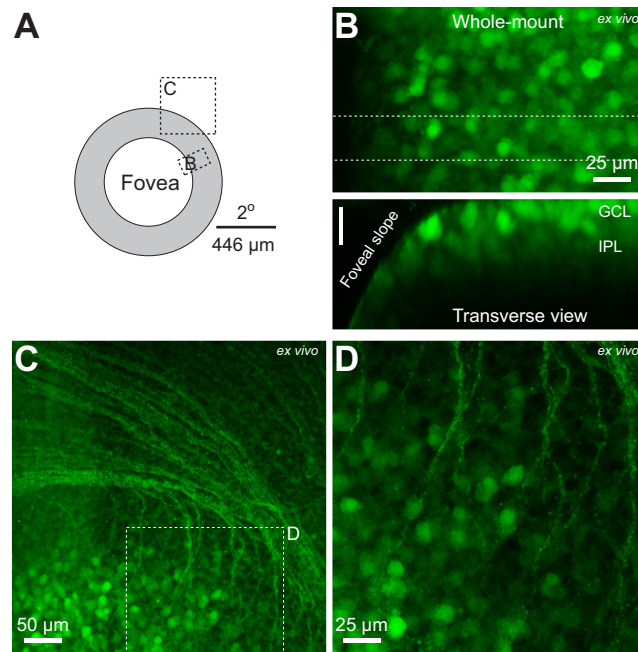


Figure 3

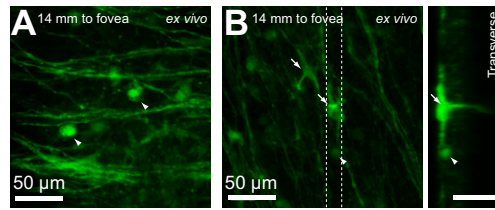


Figure 4

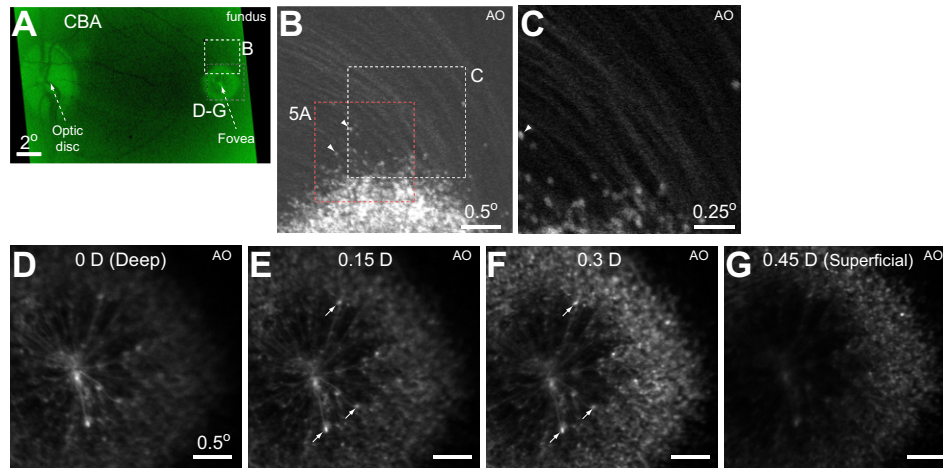


Figure 5

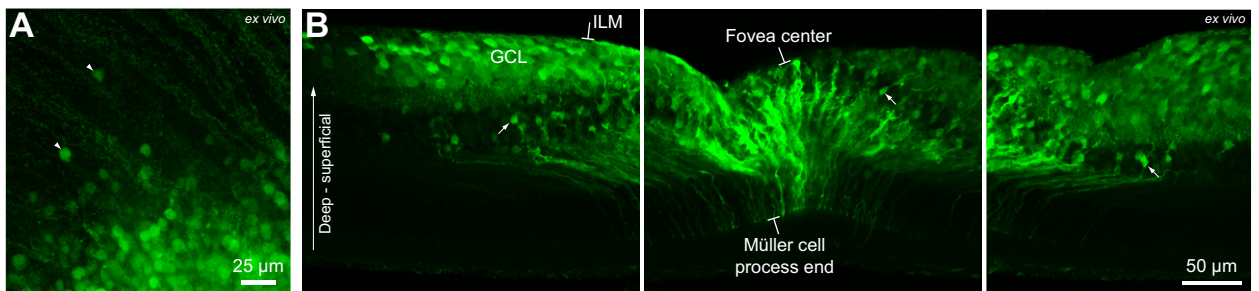


Figure 6

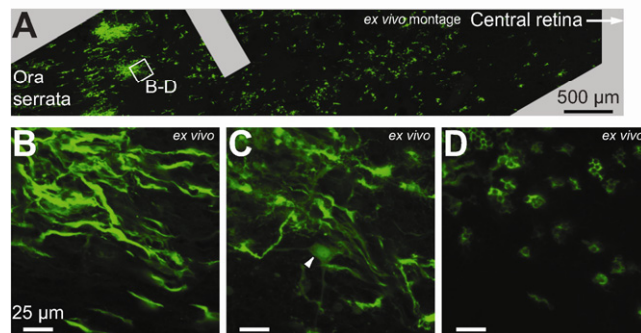


Figure 7

